

Received 17 August 2021; revised 1 November 2021; accepted 13 November 2021. Date of publication 19 November 2021;
date of current version 1 December 2021. The review of this article was arranged by Associate Editor Dr. S. Doolla.

Digital Object Identifier 10.1109/OJIA.2021.3129260

MATLAB GUI Based Steady State Open-Loop and Closed-Loop Simulation Tools for Different LLC Converters With all Operation Modes

YUQI WEI^{ID}¹ (Graduate Student Member, IEEE), ZHIQING WANG^{ID}², QUANMING LUO^{ID}² (Member, IEEE),
AND H. ALAN MANTOOTH^{ID}¹ (Fellow, IEEE)

¹ Department of Electrical Engineering, University of Arkansas, Fayetteville, AR 72701 USA

² State Key Laboratory of Power Transmission Equipment and System Security and New Technology, School of Electrical Engineering, Chongqing University, Chongqing 400044, China

CORRESPONDING AUTHOR: YUQI WEI (e-mail: yuqiwei@uark.edu)

Part of this paper was presented at the 2021 IEEE Applied Power Electronics Conference and Exposition (APEC) [15].

ABSTRACT LLC resonant converters have been widely adopted in many different industrial applications due to their characteristics of high efficiency and high power density. Simulation tools are of great importance for the analysis and design of LLC resonant converters. For example, many LLC design methods require massive simulations to finalize the circuit parameters, iterations are necessary, which can be tedious and time-consuming. Therefore, in this work, accurate and complete steady state simulation tools based on MATLAB graphical user interface (GUI) are designed for LLC resonant converters. All common and possible operation modes and LLC converter topologies are included in the designed simulation tools, which makes them practical for different applications and operation conditions. An improved mode judgement method and guidelines for initial point setting are proposed to ensure fast simulation speed. More than that, the key circuit voltage and current values are summarized for the user to evaluate the converter performance, which is more convenient than commercial simulation software. Moreover, the designed simulation tools are suitable and convenient for automatic converter parameter design.

INDEX TERMS LLC resonant converter, MATLAB GUI, simulation tool.

I. INTRODUCTION

Nowadays, efficiency and power density are two important indicators for converters. LLC resonant converters have drawn much attention since they can achieve both high efficiency and high power density conversion.

Analysis methodology plays an important role in LLC converter parameter design and system performance. Although the accuracy of conventional fundamental harmonic analysis (FHA) is high around the series resonant frequency operating point, considerable errors exist when the switching frequency is away from the series resonant frequency and the converter quality factor value is large [1]. Time domain or operation mode based analysis can be applied for LLC converters to obtain accurate results of circuit voltages and

currents [1]–[8]. The discussions of the LLC converter based on time domain analysis are all either incomplete or specific design application oriented. For example, in [2], only the discussion of PO operation mode is included, by observing the resonant inductor root-mean-square (RMS) current and transformer secondary side RMS current, the LLC converter can be optimized. Nevertheless, as discussed in [3], [4], the peak voltage gain operating point for LLC converter occurs in PN or PON mode. If only PO operation mode is considered, the regulation capability of LLC converter is not maximized. Please note that the definitions of operation modes are discussed in detail in Section II of this article. Therefore, to fully utilize the advantage of the LLC resonant tank, the design methodologies based on the peak gain point are proposed in

[5]. In [6], the operation mode analysis is presented for an LLC converter with on-board battery charger application. In [7], a computer-aided design algorithm is proposed to find the optimized circuit parameters under a given converter specification.

There are also few publications that focus on the design of simulation tools for LLC resonant converters. In [9], [10], with the aid of the time domain model and MATLAB graphical user interface (GUI) program, the simulation tools are developed for the LLC resonant converter. However, the limitations of the tools are: 1) In [9], only the PO operation mode is included. In [10], PO operation mode and NP operation mode are included in the designed GUI. The other common operation modes, including PN, PON, OPO (below resonant frequency), NOP, OP, OPO (above resonant frequency), are not included in the GUI; 2) the time domain model is derived for a full-bridge LLC converter with full-bridge rectifier, while other common LLC topologies are not included; 3) the boundary between different operation modes is not discussed.

We developed a PO operation mode based simulation tool, where the resonant capacitor and inductor ratio (the ratio between magnetizing inductor and resonant inductor) are the input parameters of the resonant tank. The simulation tool can determine the required resonant inductance and magnetizing inductance for the desired operating point [11], [12]. However, this simulation tool is not straightforward to users and only the PO operation mode is discussed.

Commercial simulation tools are also available for users, including MATLAB/SIMULINK, LTSPICE, PLECS, PSIM, SABER and so on. The issues with the commercial simulation tools are that they are not specific for LLC converter. Users must build the circuitries based on different common LLC topologies. Most importantly, the required execution time is long, which is not convenient when massive iterations are required.

Therefore, in this article, an accurate and complete time domain analysis for LLC resonant converters has been presented. For the inverter portion, there are mainly five structures: 1) full-bridge inverter; 2) symmetric half-bridge inverter; 3) asymmetric half-bridge inverter; 4) stacked structure [13]; 5) stacked structure with double frequency operation [14]. Meanwhile, there are three main structures for the rectifier portion: 1) full-bridge rectifier; 2) center-tapped transformer rectifier; 3) voltage doubler rectifier. By selecting different inverter and rectifier topologies, there are fifteen common LLC resonant converter topologies. The time domain analysis for all of these topologies is included. In addition, all the possible operation modes including PN, PON, PO, OPO (below resonant frequency), O (below resonant frequency), P, O (above resonant frequency), NP, NOP, OP, and OPO (above resonant frequency) are discussed. Moreover, to visualize and facilitate the simulation and design process, GUI programs based on MATLAB were built, including open-loop simulation and closed-loop simulation. Exactly like simulation software, by setting the converter topology and input parameters, circuit currents and voltages waveform can be drawn by using these

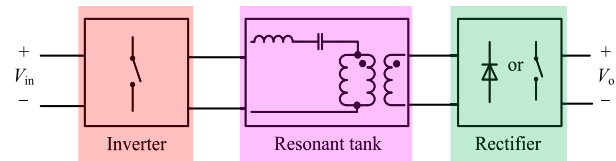


FIGURE 1. Structure of the LLC resonant converter.

GUIs. More than that, the key circuit voltage and current information are summarized for users to evaluate the converter performance. The required calculation time is displayed to evaluate the simulation speed. Lastly, these simulation tools are made open to readers so that they can download and use these tools for their own research and project.

We presented part of this work in [15], where the general time domain modelling process and simulation tool verifications are presented. Compared with [15], the following work has been included in this paper: 1) the time domain modelling process for each operation mode; 2) the boundaries between different operation modes; 3) modifications for all common LLC topologies; 4) closed-loop simulation tool is also included; 5) experiment verifications are included.; 6) lastly, the simulation tools are made open access to the readers.

The rest of this paper is organized as follows. In Section II, a general review of LLC resonant converter topologies and operation modes are presented. The time domain analysis for all LLC resonant converters and operation modes are discussed in Section III. In Section IV, introduction and verification of the designed simulation tools are implemented, which includes both the open-loop simulation tool and closed-loop simulation tool. In Section V, the experimental results from different LLC converter prototypes are presented to validate the accuracy and effectiveness of the proposed simulation tools. Finally, conclusions are drawn.

II. REVIEW FOR LLC RESONANT CONVERTER TOPOLOGIES AND OPERATION MODES

As shown in Fig. 1, an LLC resonant converter has three parts: 1) inverter; 2) LLC resonant tank; and 3) rectifier. Different LLC resonant converter topologies can be derived by selecting different inverter and rectifier structures.

A. TOPOLOGIES OF LLC RESONANT CONVERTER

For the inverter, there are mainly five structures: 1) symmetric half-bridge; 2) asymmetric half-bridge; 3) full-bridge; 4) stacked structure (stacked structure 1); 5) stacked structure with double frequency (stacked structure 2). The detailed operation of stacked structure 1 and stacked structure 2 can be found in [14].

Generally, the selection guidelines for the inverter structure can be summarized as follows: 1) symmetric and asymmetric half-bridge are suitable for low power applications; 2) full-bridge is preferred in high power applications; 3) stacked structure is recommended for high input voltage applications due to the reduced voltage stress on the primary switch; 4)

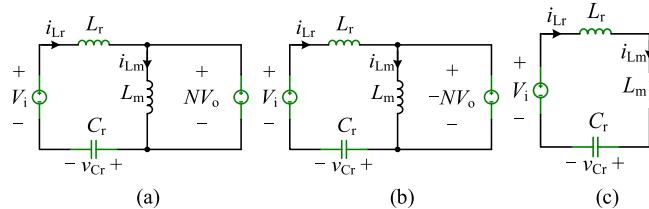


FIGURE 2. Three operation stages for LLC resonant converter. (a) P stage; (b) N stage; (c) O stage.

stacked structure with double frequency is advantageous in high input voltage and high step-down ratio applications since the input voltage magnitude is halved.

For the rectifier, there are mainly three structures: 1) full-bridge rectifier; 2) center-tapped transformer rectifier; 3) voltage doubler rectifier. The selection guidelines for the rectifier can be summarized as: 1) full-bridge rectifier can be adopted for high output voltage and low output current applications, where the voltage stress for the rectifier diode is output voltage; 2) center-tapped transformer rectifier is preferred for low output voltage and high output current applications, the reduction loss of the secondary rectifier can be significantly reduced since less diodes are required; 3) voltage doubler rectifier is suitable for step-up applications to boost the output voltage.

Based on the available inverter and rectifier structures, there exist fifteen possible LLC resonant converter topologies (five options for the inverter structure, and three options for the rectifier structure).

B. LLC OPERATION MODES

LLC resonant converter has three operation stages as shown in Fig. 2, namely P stage, O stage, and N stage. From Fig. 2(a), it can be seen that for P stage, the voltage across the magnetizing inductor is clamped by positive output voltage NV_o , and current goes through the secondary rectifier. Similarly for N stage as shown in Fig. 2(b), the voltage across the magnetizing inductor is clamped by negative output voltage $(-NV_o)$, and current goes through the secondary rectifier. While for O stage as shown in Fig. 2(c), the voltage across the magnetizing inductor is not clamped by the output voltage, and the secondary rectifier is disconnected from the transformer's primary side. Based on the sequence of these three operation stages in half switching cycle, the operation mode of the LLC resonant converter can be defined. There are eleven main operation modes for LLC resonant converter: PN, PON, PO, OPO (below resonant frequency), O (below resonant frequency), P, O (above resonant frequency), NP, NOP, OP, and OPO (above resonant frequency). For all these operation modes, they are representing the sequence of these three operation stages (P, O, and N) in half of the switching cycle. For PO operation mode, the LLC resonant converter operates in P stage first, and then followed by O stage as shown in Fig. 3(a). For PON operation mode, in half of the switching cycle, the converter is first operating in P stage, and followed by O stage, and the final stage is N stage as shown in Fig. 3(b). For PN operation

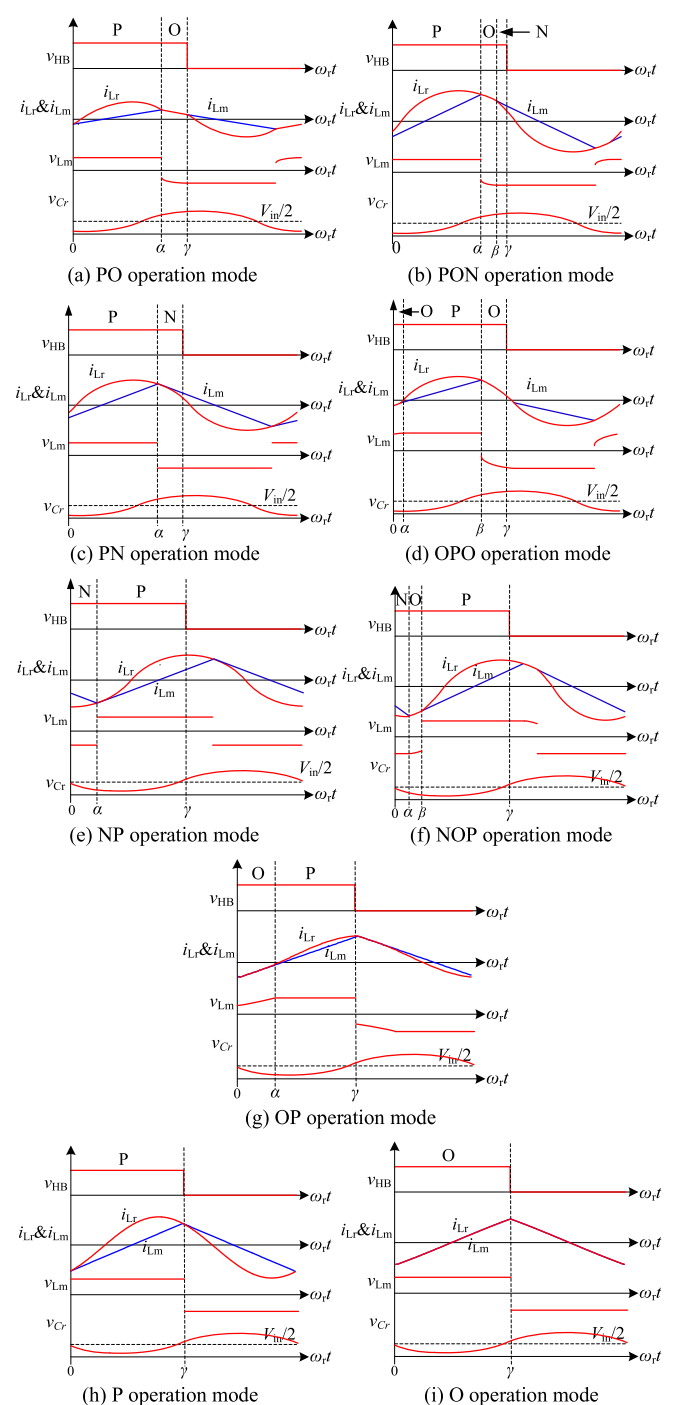


FIGURE 3. Different operation mode for LLC resonant converter.

mode, the converter is first operating in P stage and followed by N stage as shown in Fig. 3(c). For OPO operation mode, the converter is operating in O stage first, and followed by P stage, and ends with another O stage as shown in Fig. 3(d). For NP operation mode, the converter is operating in N stage first and ends with P stage as shown in Fig. 3(e). For NOP operation mode, the converter is operating in N stage first, followed by O stage and ends with P stage as shown in Fig. 3(f). For

TABLE 1. LLC Resonant Converter Operation Modes fOR LLC Resonant Converter

Switching frequency	$f_n < 1$ Low → High					$f_n = 1$	$f_n > 1$ Low → High				
Operation mode	PN	PON	PO	OPO	O	P	O	NP	NOP	OP	OPO
Voltage gain	Buck/Boost	Buck/Boost	Boost	Boost	Boost	Unity	Buck	Buck	Buck	Buck	Buck
Primary switch	ZCS/ZVS	ZCS/ZVS	ZVS	ZVS	ZVS	ZVS	ZVS	ZVS	ZVS	ZVS	ZVS
Secondary rectifier	CCM No ZCS	DCM ZCS	DCM ZCS	DCM ZCS	OFF	BCM (Boundary) ZCS	OFF	CCM No ZCS	CCM No ZCS	DCM ZCS	DCM ZCS
Output load	Heavy → Light				No load	Independent of load	No load	Heavy → Light			

Note: The peak gain frequency occurs either in PN or PON operation mode, and this explains why the voltage gain for PN or PON operation modes could be either Buck or Boost.

OP operation mode, the converter is operating in O stage first and ends with P stage as shown in Fig. 3(g). For P operation mode, during the half switching cycle, the converter is only work in P stage as shown in Fig. 3(h). For O operation mode, during the half switching cycle, only O stage occurs as shown in Fig. 3(i).

In this paper, the asymmetric half-bridge LLC resonant converter with full-bridge rectifier is selected as an example to demonstrate the operation waveforms and time domain analysis. Fig. 3 shows the operation waveforms for the LLC resonant converter with different operation modes, where v_{HB} is the half-bridge inverter output voltage, i_{Lr} is the resonant inductor current, i_{Lm} is the magnetizing inductor current, v_{Lm} is the voltage across the magnetizing inductor, and V_{Cr} is the voltage across the resonant capacitor. Please note that the operation waveforms for OPO and O operation mode in both the below resonant frequency and above resonant frequency region are the same. PON, PN, and PO operation modes occur when the switching frequency is lower than the series resonant frequency, while NP, NOP, OP operation modes happen when the switching frequency is higher than the series resonant frequency. The OPO operation mode occurs over the entire switching frequency region with low output power. The P operation mode occurs when the switching frequency equals the series resonant frequency. And O operation mode occurs over the entire switching frequency range with no load. The half switching period is denoted as γ , and the end of the first stage is denoted as α , while the end of the second stage is denoted as β . The detailed mathematical derivations and operation mode boundaries for different operation mode are presented in next Section.

III. MATHEMATICAL DERIVATIONS FOR DIFFERENT OPERATION MODES

There are two assumptions for the modelling: 1) the converter is operating in steady state condition; 2) ideal components are assumed or the circuit parasitics are ignored.

Table 1 summarizes the distribution of different operation modes for an LLC resonant converter. The voltage gain, soft switching operation for semiconductors, and output power are summarized. As discussed in [3], the LLC converter peak gain

operating point occurs either in PN or PON operation mode, so the voltage gain in these two operation modes could be either Buck or Boost. When the switching frequency is in the range of the peak gain frequency and unity normalized switching frequency, the voltage gain is boosted with the decrease of the switching frequency. Another important observation is that O stage occurs when the output power is decreased, since there is no power transferred to the load during the O stage. In this section, the mathematical derivations for each operation mode and the boundary conditions between different operation modes are presented. In addition, because the mathematical derivation discussed in this section is based on the asymmetric half-bridge inverter with full-bridge rectifier, the required modifications of the model for other LLC resonant converter topologies are also summarized.

A. MATHEMATICAL DERIVATIONS FOR THREE OPERATION STAGES

Before discussing the derivations, some definitions of the LLC resonant converter are summarized in Table 2.

Due to the symmetric characteristic of the positive and negative half-cycle of the converter, only half of the switching period is analyzed. Generally, there are three possible resonant stages during half period as shown in Fig. 2. These are denoted as P, O and N, respectively. Then, based on the normalization of the resonant unit, different resonant stages can be described mathematically as follows [6].

The P resonant stage, is characterized by the positive polarity of magnetizing inductor voltage, namely, the resonant inductor L_r is in resonance with the resonant capacitor C_r as shown in Fig. 2(a). The normalized resonant capacitor voltage, resonant inductor current, magnetizing inductor current, and magnetizing inductor voltage for this stage can be respectively described as (1). Based on the Kirchhoff's voltage law (KVL), the P stage can be modelled with a second-order differential equation. Then, the expressions for the normalized resonant capacitor voltage and normalized resonant inductor current can be derived by solving the second order differential equation.

$$j_{LrP}(\theta) = j_{Lr}(\theta_{ini}) \cdot \cos(\theta - \theta_{ini})$$

TABLE 2. LLC Converter Definitions

Angular series resonant frequency ω_r	$\omega_r = \frac{1}{\sqrt{L_r C_r}}$
Angular parallel resonant frequency ω_m	$\omega_m = \frac{1}{\sqrt{(L_r + L_m)C_r}}$
Operation angle θ	$\theta = \omega_r t$
Normalized switching frequency F	$F = \frac{\omega_s}{\omega_r}$
Half period switching cycle γ	$\gamma = \frac{\omega_r}{2f_s}$
Converter voltage gain m	$m = \frac{nV_o}{V_i}$
Normalized voltage V_{base}	$V_{base} = nV_o$
Normalized impedance Z_{base}	$Z_{base} = \sqrt{\frac{L_r}{C_r}}$
Normalized current I_{base}	$I_{base} = \frac{V_{base}}{Z_{base}}$
Normalized resonant capacitor voltage $m_{Cr}(\theta)$	$m_{Cr}(\theta) = \frac{V_{Cr}(\theta)}{V_{base}}$
Normalized magnetizing inductor voltage $m_{Lm}(\theta)$	$m_{Lm}(\theta) = \frac{V_{Lm}(\theta)}{V_{base}}$
Normalized resonant inductor voltage $m_{Lr}(\theta)$	$m_{Lr}(\theta) = \frac{V_{Lr}(\theta)}{V_{base}}$
Normalized resonant inductor current $j_{Lr}(\theta)$	$j_{Lr}(\theta) = \frac{i_{Lr}(\theta)}{I_{base}}$
Normalized magnetizing inductor current $j_{Lm}(\theta)$	$j_{Lm}(\theta) = \frac{i_{Lm}(\theta)}{I_{base}}$
Normalized output current j_{out}	$j_{out} = \frac{i_{out}}{I_{base}}$
Normalized output load resistance r_L	$r_L = \frac{N^2 R_L}{Z_{base}}$
Inductor ratio λ	$\lambda = \frac{L_r}{L_m}$
Ratio of two resonant frequencies k_1	$k_1 = \frac{\omega_m}{\omega_r}$

$$+ [1/m - 1 - m_{Cr}(\theta_{ini})] \cdot \sin(\theta - \theta_{ini})$$

$$j_{LmP}(\theta) = j_{Lm}(\theta_{ini}) + \lambda \cdot (\theta - \theta_{ini})$$

$$m_{LmP}(\theta) = 1$$

$$m_{CrP}(\theta) = 1/m - 1 - [1/m - 1 - m_{Cr}(\theta_{ini})] \cdot \cos(\theta - \theta_{ini}) \\ + j_{Lr}(\theta_{ini}) \cdot \sin(\theta - \theta_{ini}) \quad (1)$$

Similarly, the voltage across the magnetizing inductor is negatively clamped by the output voltage for the N resonant stage as shown in Fig. 2(b), which can be described as

$$j_{LrN}(\theta) = j_{Lr}(\theta_{ini}) \cdot \cos(\theta - \theta_{ini}) \\ + [1/m + 1 - m_{Cr}(\theta_{ini})] \cdot \sin(\theta - \theta_{ini})$$

$$j_{LmN}(\theta) = j_{Lm}(\theta_{ini}) - \lambda \cdot (\theta - \theta_{ini})$$

$$m_{LmN}(\theta) = -1$$

$$m_{CrN}(\theta) = 1/m + 1 - [1/m + 1 - m_{Cr}(\theta_{ini})] \cdot \cos(\theta - \theta_{ini}) \\ + j_{Lr}(\theta_{ini}) \cdot \sin(\theta - \theta_{ini}) \quad (2)$$

Since the O resonant stage happens when no power flows to the secondary side of the transformer, it forces the magnetizing inductor to join the resonant unit as shown in Fig. 2(c), and the normalized resonant frequency becomes $k_1 \cdot \theta$. Then the stage equations can be expressed as

$$j_{LrO}(\theta) = j_{Lr}(\theta_{ini}) \cdot \cos[k_1 \cdot (\theta - \theta_{ini})] \\ + k_1 \cdot [1/m - m_{Cr}(\theta_{ini})] \cdot \sin[k_1 \cdot (\theta - \theta_{ini})]$$

$$j_{LmO}(\theta) = j_{Lm}(\theta)$$

$$m_{LmO}(\theta) = [-m_{CrO}(\theta_{ini}) + 1/m]/(1 + \lambda)$$

$$m_{CrO}(\theta) = 1/m - [1/m - m_{Cr}(\theta_{ini})] \cdot \cos[k_1 \cdot (\theta - \theta_{ini})] \\ + j_{Lr}(\theta_{ini})/k_1 \cdot \sin[k_1 \cdot (\theta - \theta_{ini})] \quad (3)$$

It is noted that θ_{ini} represents the initial angle of the stage, and the initial value of the resonant capacitor voltage, resonant inductor current and magnetizing inductor current can be described as $j_{Lr}(0)$, $j_{Lm}(0)$, and $m_{Cr}(0)$, respectively.

Different operation modes can be obtained by combining these three operation stages in the half switching period. Then, mathematical derivations for the different operation modes are discussed.

B. MATHEMATICAL DERIVATIONS FOR DIFFERENT OPERATION MODES

1) PO OPERATION MODE (FIG. 3(A))

During the P stage ($0 \leq \theta \leq \alpha$), the following circuit stage equations can be given by (1).

$$j_{Lr}(\theta) = j_{Lr}(0) \cdot \cos(\theta) + [1/m - 1 - m_{Cr}(0)] \cdot \sin(\theta)$$

$$j_{Lm}(\theta) = j_{Lm}(0) + \lambda \cdot \theta$$

$$m_{Lm}(\theta) = 1$$

$$m_{Cr}(\theta) = 1/m - 1 - [1/m - 1 - m_{Cr}(0)] \cdot \cos(\theta) \\ + j_{Lr}(0) \cdot \sin(\theta) \quad (4)$$

Then, during O stage 1 ($\alpha \leq \theta \leq \gamma$), it can be described as

$$j_{Lr}(\theta) = j_{Lr}(\alpha) \cdot \cos[k_1 \cdot (\theta - \alpha)] \\ + k_1 \cdot (1/m - m_{Cr}(\alpha)) \cdot \sin[k_1 \cdot (\theta - \alpha)]$$

$$j_{Lm}(\theta) = j_{Lm}(\theta)$$

$$m_{Lm}(\theta) = [-m_{CrO}(\alpha) + 1/m]/(1 + \lambda)$$

$$m_{Cr}(\theta) = 1/m - [1/m - m_{Cr}(\alpha)] \cdot \cos[k_1 \cdot (\theta - \alpha)] \\ + j_{Lr}(\alpha)/k_1 \cdot \sin[k_1 \cdot (\theta - \alpha)] \quad (5)$$

Due to the characteristics of the circuit, there are three constraints for each operation mode. The first one is the continuity of the resonant capacitor voltage, resonant inductor current, and magnetizing inductor current. This means the

value of these stage variables at the switching instant between two stages can be calculated by either stage equation and the results are equal. The second constrain is the symmetry of the resonant capacitor voltage, resonant inductor current, magnetizing inductor current. This means the initial value and end value of these three variables are opposite (for asymmetric half-bridge inverter structure, the resonant capacitor voltage is symmetric with $V_i/2$), namely, $j_{Lr}(0) = -j_{Lr}(\gamma)$, $j_{Lm}(0) = -j_{Lm}(\gamma)$, $m_{Cr}(0) + m_{Cr}(\gamma) - 1/m = 0$. The third constrain is the law of energy conservation, that is, the system efficiency is assumed to be 100%. During one switching period, the input energy equals the output energy, which can be expressed as

$$j_{out} = \frac{1}{\gamma} \int_0^\gamma |j_{Lr}(\theta) - j_{Lm}(\theta)| d\theta = 1/r_L \quad (6)$$

Thus, based on the above three constrains, the following equations for PO mode can be obtained.

$$\begin{cases} j_{Lr}(0) - j_{Lm}(0) = 0 \\ j_{Lr}(\alpha) - j_{Lm}(\alpha) = 0 \\ m_{Cr}(0) + m_{Cr}(\gamma) - \frac{1}{m} = 0 \\ j_{Lr}(0) + j_{Lr}(\gamma) = 0 \\ j_{out} r_L - 1 = 0 \end{cases} \quad (7)$$

For open-loop simulation, there are five unknown parameters in (7), namely, $j_{Lr}(0)$, $j_{Lm}(0)$, $m_{Cr}(0)$, the end phase angle of P stage α and the voltage gain m . These can be solved by the above five equations. Similarly, for closed-loop simulation, the voltage gain m becomes input parameter, the five unknown parameters are $j_{Lr}(0)$, $j_{Lm}(0)$, $m_{Cr}(0)$, the end phase angle of P stage α and the switching frequency f_s . Here, a numerical-based computation tool is required, and MATLAB is selected in this paper. Similarly, based on the continuity condition, symmetrical condition, and the law of energy conservation, the quantitative calculation of other resonant modes can be done with the stage variables expressed by (1), (2), and (3).

2) PON OPERATION MODE (FIG. 3(B))

For PON operation mode, the duration for O stage β is unknown. Therefore, one more equation is required. Due to the continuity condition, the voltage across the magnetizing inductor m_{Lm} at the end of O stage is equal to that at the beginning of N stage. One more equation can be added into (7). Besides, the magnetizing inductor current and resonant inductor current are not equal at the initial angle, so this equation in (7) should be removed, and the symmetrical condition of the magnetizing inductor current can be added, which can be expressed as

$$\begin{cases} j_{Lm}(0) + j_{Lm}(\gamma) = 0 \\ j_{Lr}(\alpha) - j_{Lm}(\alpha) = 0 \\ m_{Cr}(0) + m_{Cr}(\gamma) - \frac{1}{m} = 0 \\ j_{Lr}(0) + j_{Lr}(\gamma) = 0 \\ m_{Lm}(\beta) + 1 = 0 \\ j_{out} r_L - 1 = 0 \end{cases} \quad (8)$$

3) PN OPERATION MODE (FIG. 3(C))

For PN operation mode, the equations can be obtained based on that of PON mode. The equation derived by the O stage should be removed, and obtaining

$$\begin{cases} j_{Lm}(0) + j_{Lm}(\gamma) = 0 \\ j_{Lr}(\alpha) - j_{Lm}(\alpha) = 0 \\ m_{Cr}(0) + m_{Cr}(\gamma) - \frac{1}{m} = 0 \\ j_{Lr}(0) + j_{Lr}(\gamma) = 0 \\ j_{out} r_L - 1 = 0 \end{cases} \quad (9)$$

4) OPO OPERATION MODE (FIG. 3(D))

For OPO operation mode, the duration for the P stage β is unknown. Based on the operation mode waveform, at the beginning of the second O stage, the resonant inductor current $i_{Lr}(\beta)$ equals the magnetizing inductor current $i_{Lm}(\beta)$, while the condition $i_{Lr}(0) = i_{Lm}(0)$ is equivalent to $i_{Lr}(\alpha) = i_{Lm}(\alpha)$ during the first O stage. Thus, one of the equations in (7) should be removed, and one more equation should be added. That is, the voltage across the magnetizing inductor m_{Lm} at the switching angle between the first O stage and the P stage is continuous. The non-linear equations for OPO operation mode can be expressed as

$$\begin{cases} m_{Lm}(\alpha) - 1 = 0 \\ j_{Lr}(\alpha) - j_{Lm}(\alpha) = 0 \\ m_{Cr}(0) + m_{Cr}(\gamma) - \frac{1}{m} = 0 \\ j_{Lr}(0) + j_{Lr}(\gamma) = 0 \\ j_{Lr}(\beta) - j_{Lm}(\beta) = 0 \\ j_{out} r_L - 1 = 0 \end{cases} \quad (10)$$

5) NP OPERATION MODE (FIG. 3(E))

For NP operation mode, these constrains are equivalent to that of PN mode, which can also be expressed by (9).

6) NOP OPERATION MODE (FIG. 3(F))

Similar to PON mode, the equations of NOP mode can be derived by the symmetrical condition of the three state variables: the continuity condition of the voltage across the magnetizing inductor m_{Lm} at β , the switching angle between O stage and P stage, and the law of energy conservation. Then, the non-linear equations for NOP operation mode can be expressed as

$$\begin{cases} j_{Lm}(0) + j_{Lm}(\gamma) = 0 \\ j_{Lr}(\alpha) - j_{Lm}(\alpha) = 0 \\ m_{Cr}(0) + m_{Cr}(\gamma) - \frac{1}{m} = 0 \\ j_{Lr}(0) + j_{Lr}(\gamma) = 0 \\ m_{Lm}(\beta) - 1 = 0 \\ j_{out} r_L - 1 = 0 \end{cases} \quad (11)$$

7) OP OPERATION MODE (FIG. 3(G))

For OP operation mode, since the resonant inductor current equals the magnetizing inductor current during the O stage, the constrains of $i_{Lr}(0) = i_{Lm}(0)$ or $i_{Lr}(\alpha) = i_{Lm}(\alpha)$ in (7) should be removed, and the symmetrical condition of the magnetizing

TABLE 3. Modifications for Different LLC Resonant Converter Topologies

	Asymmetric half-bridge inverter	Symmetric half-bridge inverter	Full-bridge inverter	Stacked structure 1	Stacked structure 2
Full-bridge rectifier	No modification	V_{Cr} is shifted down by $V_i/2$	V_{Cr} is shifted down by $V_i/2$; $i_{Ls}, i_{Lm}, i_D, V_{Cr}$ and V_o are doubled.	No modification	The input voltage is modified as: $V_i = V_i/2$; The switching frequency is modified as: $f_s = 2f_s$.
Center-tapped transformer	No modification	V_{Cr} is shifted down by $V_i/2$	V_{Cr} is shifted down by $V_i/2$; $i_{Ls}, i_{Lm}, i_D, V_{Cr}$ and V_o are doubled.	No modification	The input voltage is modified as: $V_i = V_i/2$; The switching frequency is modified as: $f_s = 2f_s$.
Voltage doubler rectifier	The load resistance is modified as: $R_L = R_L/4$; The output voltage is doubled.	V_{Cr} is shifted down by $V_i/2$; The load resistance is modified as: $R_L = R_L/4$; The output voltage is doubled.	The load resistance is modified as: $R_L = R_L/4$; V_{Cr} is shifted down by $V_i/2$; $i_{Ls}, i_{Lm}, i_D, V_{Cr}$ and V_o are doubled; The output voltage is four-fold.	The load resistance is modified as: $R_L = R_L/4$; The output voltage is doubled.	The input voltage is modified as: $V_i = V_i/2$; The switching frequency is modified as: $f_s = 2f_s$. The load resistance is modified as: $R_L = R_L/4$; The output voltage is doubled.

inductor current can be added, which can be expressed as

$$\begin{cases} j_{Lm}(0) + j_{Lm}(\gamma) = 0 \\ j_{Lr}(\alpha) - j_{Lm}(\alpha) = 0 \\ m_{Cr}(0) + m_{Cr}(\gamma) - \frac{1}{m} = 0 \\ j_{Lr}(0) + j_{Lr}(\gamma) = 0 \\ j_{out} r_L - 1 = 0 \end{cases} \quad (12)$$

8) P OPERATION MODE (FIG. 3(H))

For P operation mode, there is only one stage, the equation regarding the resonant inductor current equals the magnetizing inductor current at α in (7) can be removed, so

$$\begin{cases} j_{Lr}(0) - j_{Lm}(0) = 0 \\ m_{Cr}(0) + m_{Cr}(\gamma) - \frac{1}{m} = 0 \\ j_{Lr}(0) + j_{Lr}(\gamma) = 0 \\ j_{out} r_L - 1 = 0 \end{cases} \quad (13)$$

9) O OPERATION MODE (FIG. 3(I))

The same equation in P operation mode can be used to solve the O operation mode according to the operational principles in Fig. 3(h) and Fig. 3(i).

Based on the above equations, the converter in different modes can be completely calculated.

C. MODIFICATIONS FOR DIFFERENT LLC RESONANT CONVERTER TOPOLOGIES

As stated previously, the above analysis is implemented based on the asymmetric half-bridge inverter structure with full-bridge rectifier. When different LLC resonant converter topologies are selected, some necessary modifications are required correspondingly. 1) Inverter: for full-bridge inverter structure, all the circuit voltages and currents are doubled, and since the inverter output voltage is symmetric with zero, the resonant capacitor voltage waveform should be shifted down by $V_i/2$. For the symmetric half-bridge inverter, only the resonant capacitor voltage waveform should be shifted down by $V_i/2$. For the stacked structure 1, its operation is the same

as the asymmetric half-bridge, so no modification is required. For the stacked structure 2, the switching frequency should be modified as $2f_s$ due to its double frequency operation, and the input voltage should be modified as $V_i/2$ since the magnitude of the inverter output voltage is $V_i/2$. 2) Rectifier: for the center-tapped transformer rectifier structure, no modification is required. For the voltage doubler rectifier structure, the load resistance is modified as $R_L/4$ since the voltage is doubled, which means the equivalent power is four-fold. The modifications for different LLC resonant converter topologies are summarized in Table 3.

D. BOUNDARY CONDITIONS BETWEEN DIFFERENT OPERATION MODES

Traditionally, the boundary condition between different modes is defined by the magnetizing inductor voltage m_{Lm} [7]. However, because of the abrupt change of the voltage at the switching angle between two resonant stages, the accuracy of the judgement is reduced. Since the solver of the converter and the mode judgement is based on the initial assumption, a false assumption will lead to false calculation results and judgement. To address these problems, in this paper, the judgement is carried out at an angle slightly greater than the switching angle between two stages, and the result will not output until it is consistent with the assumption. The flow chart of the judgement is presented in Fig. 4.

PO, PON, and PN modes exist in the region that the switching frequency is below the resonant frequency, namely, $F < 1$. OP, NOP, NP modes exist in the region of $F > 1$, and OPO mode exists over the whole operation range. The P operation mode exists when $F = 1$ and O operation mode exists when there is no output power. The judgement can be classified into two main parts by the normalized frequency F , as is shown in Fig. 4. When $F < 1$, the LLC unit is assumed to operate in PN mode first. If the assumption is true, the resonant unit is in P stage during the first subinterval, and the resonant inductor current should be greater than the magnetizing inductor current, namely, $j_{Lr}(0) > j_{Lm}(0)$. During the second subinterval,

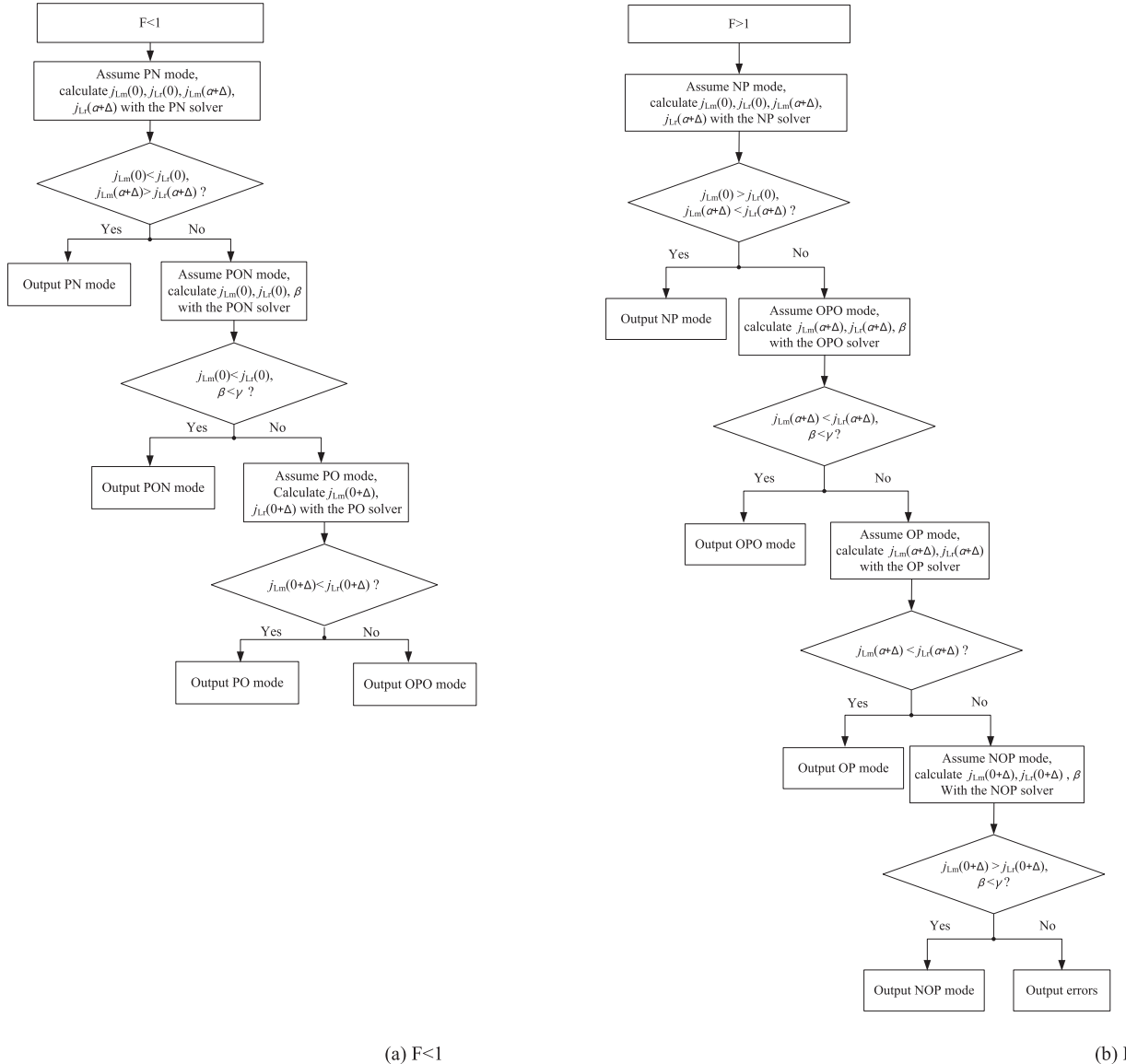


FIGURE 4. Boundary condition for different operation modes.

when the resonant unit enters N stage, $j_{Lr}(\theta) < j_{Lm}(\theta)$ should be satisfied. And an angle slightly greater than the switching angle between P stage and N stage is selected for the verification of the second resonant stage, which is expressed as $j_{Lr}(\alpha+\Delta) < j_{Lm}(\alpha+\Delta)$, where Δ is the small angle increase. Thus, if both the relationships between the two inductor currents are satisfied, the assumption of PN is true, and it will output. Otherwise, it is assumed to be operating in PON mode. The resonant inductor current should be greater than the magnetizing inductor current at the initial angle for PON mode as shown in Fig. 3(b), while these two currents are equal at the initial angle in PO mode as shown in Fig. 3(a). This characteristic is used as the first condition for the verification of PON mode. The end angle of second subinterval β should be smaller than the half period γ , so it is taken as the second condition for PON mode. Thus, if both the inductor current relationship and the angle condition are satisfied, the PON

mode will output. Otherwise, the PO mode is assumed to be true. To distinguish between this mode and OPO mode, the two inductor currents at the angle $(0+\Delta)$ should be compared. For PO mode, the resonant inductor current should be greater than the magnetizing inductor current at this angle, otherwise, the OPO mode is true. Similarly, when $F > 1$, the converter can be solved by assumptions and verifications. It is noteworthy to mention that in this operation region, the OP mode and NOP mode exist in the narrow range. Thus, to expedite calculation speed, the converter is assumed to operate in NP mode first, if the condition for NP mode is not satisfied, then the assumption of OPO mode is made.

IV. INTRODUCTION AND VERIFICATION OF THE DESIGNED SIMULATION TOOLS

In Section III, the mathematical derivations and operation boundaries for different operation modes are discussed. Based

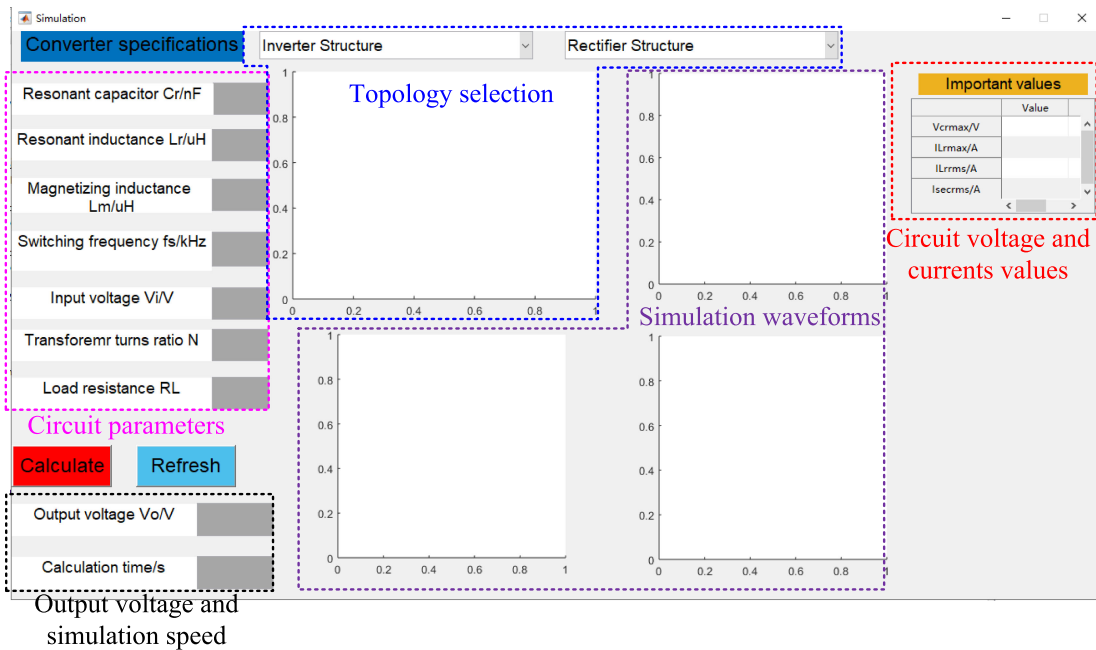


FIGURE 5. The designed MATLAB GUI program for open-loop simulation tool.

on these discussions, GUI programs based on MATLAB were built to simulate the LLC resonant converter in both open-loop form and closed-loop form. The simulation speed is less than two seconds during the whole operation region. Introduction and verification of the designed simulation tools are presented in this Section. Please note that although only one complete cycle is demonstrated in the designed simulation tool, the number of cycles can be displayed is not restricted. During the steady state operation, the waveforms are exactly same for each cycle. Simulation result with two complete cycles is presented in the uploaded multimedia.

A. INTRODUCTION OF THE DESIGNED OPEN-LOOP SIMULATION TOOL

Fig. 5 shows the interface of the designed simulation tool for the LLC resonant converter. It mainly includes the following five parts: 1) topology selection: as discussed in Section II, an LLC resonant converter has fifteen topologies based on different combinations of the inverter and rectifier structures, the picture of the topology will be shown in the figure area; 2) circuit parameters: like the traditional simulation software, the circuit parameters including LLC resonant tank parameters, transformer turns ratio, switching frequency, input voltage, and load resistance are required to initiate the simulation; 3) output voltage and simulation speed: based on the mathematical model discussed in Section III, the output voltage can be obtained. To evaluate the simulation speed, the calculation time is displayed; 4) simulation waveforms: after solving the LLC resonant converter, the key waveforms in steady state, resonant inductor current, magnetizing inductor current, resonant capacitor voltage, and secondary rectifier diode current, are plotted; 5) circuit voltage and current

values: when designing an LLC resonant converter, the following circuit voltage and current values are important to designers: maximum voltage of resonant capacitor (it is important for the resonant capacitor selection), maximum resonant inductor current (it is important for the primary switch selection-current stress), RMS values for resonant inductor current and transformer secondary current (it is important for converter power loss analysis).

B. VERIFICATION OF THE DESIGNED OPEN-LOOP SIMULATION TOOL

To verify the accuracy and effectiveness of the designed simulation tool for the LLC resonant converter, comparisons between the results from the designed simulation tool and commercial simulation software PSIM are made in this Section. The comparisons include some key operation modes. Please note that the simulation verifications for other operation modes are presented in the uploaded multimedia. The asymmetric half-bridge inverter with center-tapped transformer rectifier structure is selected as an example. By ignoring the circuit parasitics and using ideal components in PSIM, the results obtained from the developed simulation tools are exactly same as the PSIM simulation results. It is unable to see any differences between these two results by drawing them in the same figures. To demonstrate the differences between the PSIM simulation results and designed simulation tool, some key circuit parasitics are added. The parasitics considered in the simulations are summarized in Table 4. Please note that due to the size of the screenshot, the important values on the top right side are removed to make other part readable. The complete screenshots are also provided in the uploaded multimedia.

TABLE 4. Circuit Parameters Used in the Designed Tool and PSIM Simulation Software

Circuit symbol	Parameters in the designed tool	Parameters in PSIM simulation
Primary MOSFET	Ideal	On-state resistance: 50 mΩ Junction capacitance: 200 pF
Secondary rectifier	Ideal	Forward voltage drop: 0.5 V Dynamic resistance: 40 mΩ
Deadtime	-	0.05 s
Resonant capacitor C_r	66 nF	66 nF
Resonant inductor L_r	38 μH	38 μH Series resistance: 50 mΩ
Magnetizing inductor L_m	200 μH	200 μH Primary series resistance: 50 mΩ Secondary series resistance: 50 mΩ
Transformer turns ratio N	4	4
Input voltage V_i/V	380 V	380 V

1) PO OPERATION MODE ($R_L=10 \Omega$, $F_s=50 \text{ KHZ}$)

Compared with PN and PON operation modes, by further increasing the load resistance value, the LLC resonant converter will operate in PO operation mode. Fig. 6 shows the comparison results in PO operation mode.

2) OPO OPERATION MODE ($R_L=20 \Omega$, $F_s=50 \text{ KHZ}$)

The LLC resonant converter will operate in OPO operation mode when the load resistance value increases or output power decreases. Fig. 7 shows the comparison results in OPO operation mode.

3) NP OPERATION MODE ($R_L=5 \Omega$, $F_s=120 \text{ KHZ}$)

NP operation mode occurs when the switching frequency is higher than the series resonant frequency with low resistance. Fig. 8 shows the comparison results in NP operation mode.

4) NOP OPERATION MODE ($R_L=20 \Omega$, $F_s=120 \text{ KHZ}$)

NOP operation mode occurs when the switching frequency is higher than the series resonant frequency with large resistance. Fig. 9 shows the comparison results in NOP operation mode.

From Figs. 6 to 9, one can observe that even by taking the circuit parasitics into considerations, the accuracy of the developed simulation tool is still very high, which can be beneficial and applied for the analysis and design of the LLC converters.

C. INTRODUCTION OF THE DESIGNED CLOSED-LOOP SIMULATION TOOL

Similar to the open-loop simulation tool, Fig. 10 shows the interface of the designed closed-loop simulation tool. For the closed-loop simulation, the users can select three different closed-loop simulation types, namely, output voltage, output current, and output power. The only difference is that for the closed-loop simulation tool, the output voltage/output current/output power is known parameter and

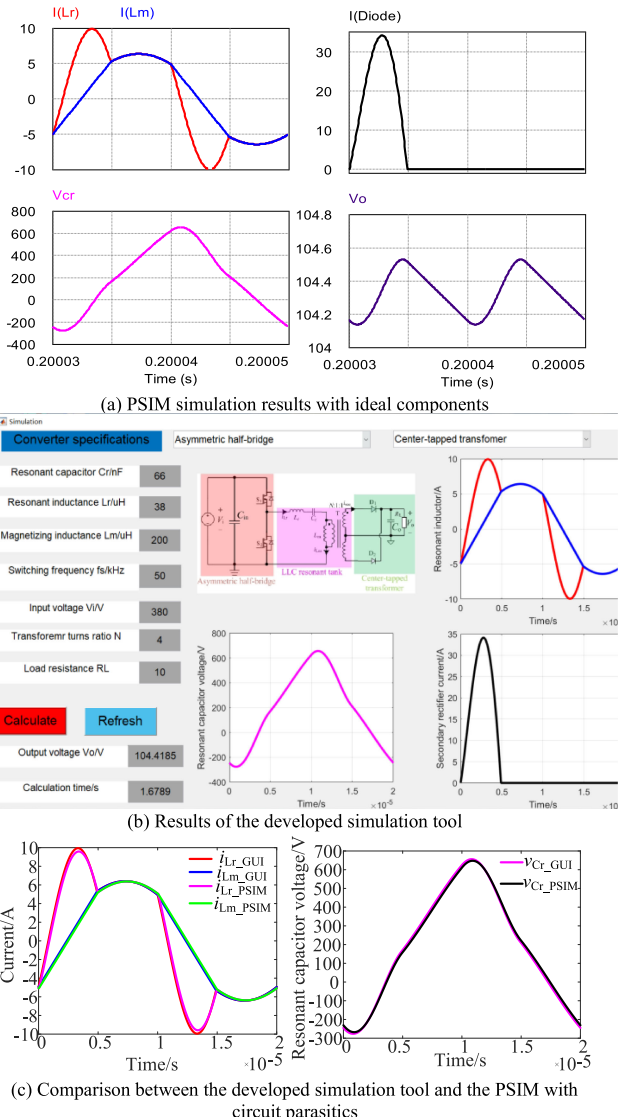
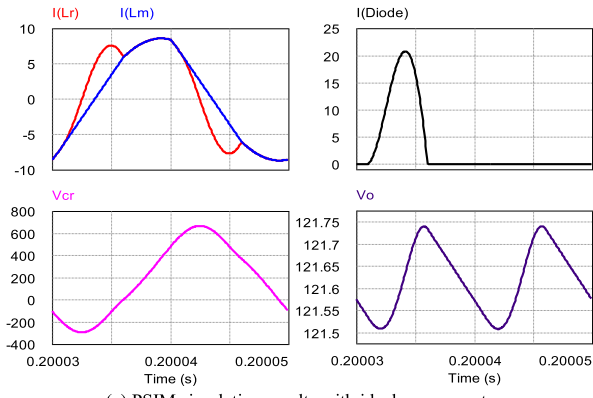


FIGURE 6. PO operation mode.

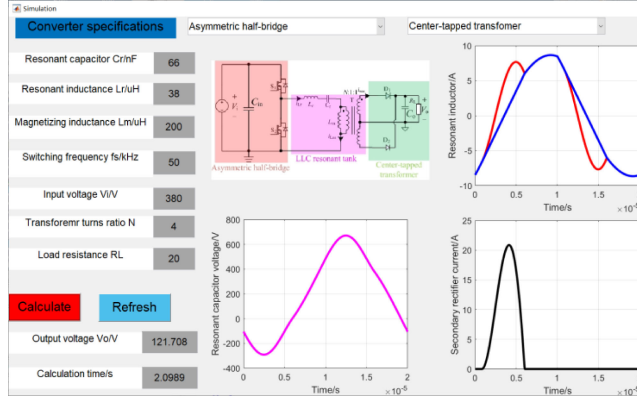
switching frequency is the unknown parameter, while for the open-loop simulation tool, the output voltage/output current/output power is unknown parameter and switching frequency is known parameter. Another difference between the open-loop simulation and closed-loop simulation is the mode judgement. For the closed-loop simulation tool, instead of the normalized switching frequency F , the converter voltage gain m is used to divide the converter operation in below resonant frequency ($m>1$), at resonant frequency ($m=1$), and above resonant frequency ($m<1$).

D. VERIFICATION OF THE DESIGNED CLOSED-LOOP SIMULATION TOOL

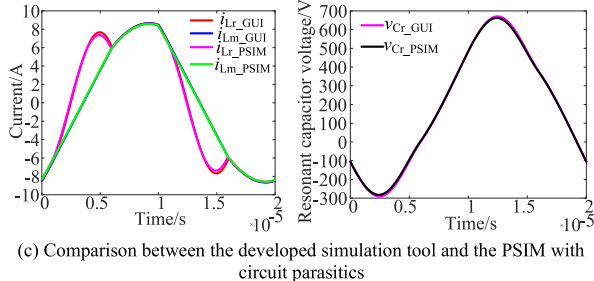
In this part, only some common operation modes including PO, OPO, P, and NP operation modes are selected to validate the accuracy and effectiveness of the designed closed-loop simulation tool. The asymmetric half-bridge inverter with



(a) PSIM simulation results with ideal components



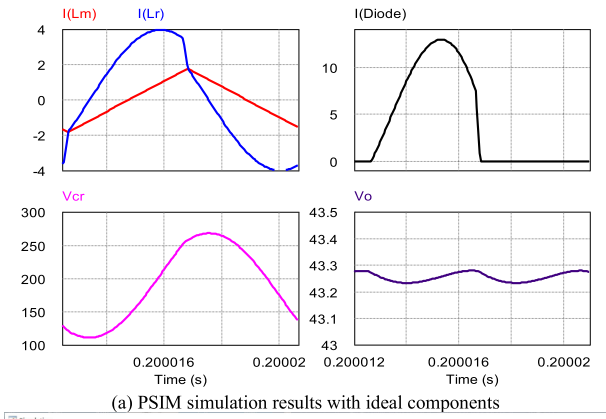
(b) Results of the developed simulation tool

**FIGURE 7.** OPO operation mode.

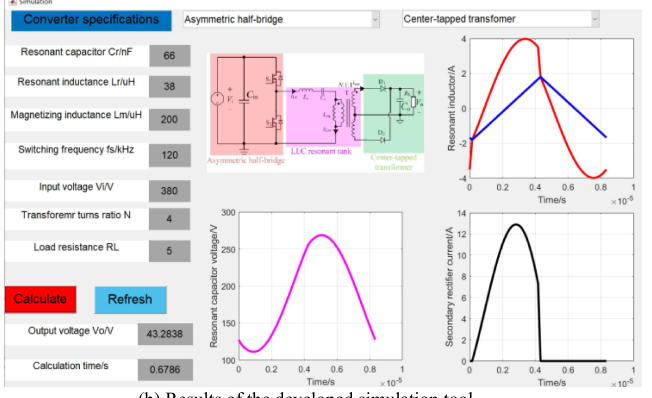
full-bridge rectifier LLC topology is selected, and the circuit parameters are: $C_r=35.2\text{ nF}$, $L_r=72\text{ }\mu\text{H}$, $L_m=346\text{ }\mu\text{H}$, $N=3.8$, $V_o=48\text{ V}$. Please note that ideal components are used in the simulation for comparison purpose. The results obtained from the developed simulation tool agree completely with the PSIM results without considering the circuit parasitics.

1) PO OPERATION MODE ($V_i=280\text{ V}$, $R_L=12\text{ }\Omega$)

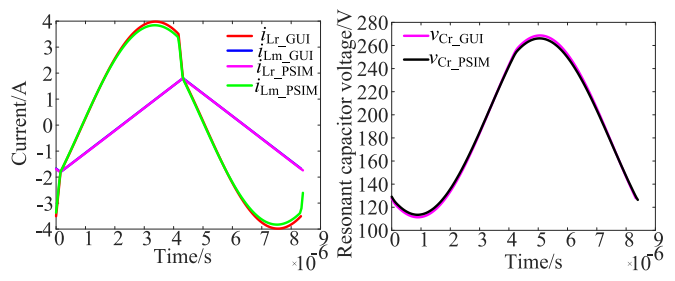
Under these circuit parameters, the LLC converter is operating in PO operation mode, and the calculated required switching frequency is 64.645 kHz. By designing the switching frequency as 64.645 kHz, the simulation waveforms are presented to validate the accuracy of the designed closed-loop simulation tool as shown in Fig. 11. With the calculated switching frequency, the output voltage of the simulation is 48 V as desired.



(a) PSIM simulation results with ideal components



(b) Results of the developed simulation tool



(c) Comparison between the developed simulation tool and the PSIM with circuit parasitics

FIGURE 8. NP operation mode.

2) OPO OPERATION MODE ($V_i=280\text{ V}$, $R_L=30\text{ }\Omega$)

When the output power is decreased, the converter is operating in OPO operation mode. The simulation results obtained from PSIM and the designed closed-loop simulation software are shown in Fig. 12.

3) P OPERATION MODE ($V_i=364\text{ V}$, $R_L=12\text{ }\Omega$)

The resonant frequency point operation is achieved at $V_i=364\text{ V}$ as shown in Fig. 13.

4) NP OPERATION MODE ($V_i=380\text{ V}$, $R_L=12\text{ }\Omega$)

When the input voltage is greater than 364 V, the LLC converter is operating in above resonant frequency region, with $R_L=12\text{ }\Omega$, the converter is operating in NP operation mode. Fig. 14 shows the simulation results from PSIM and the designed closed-loop simulation tool.

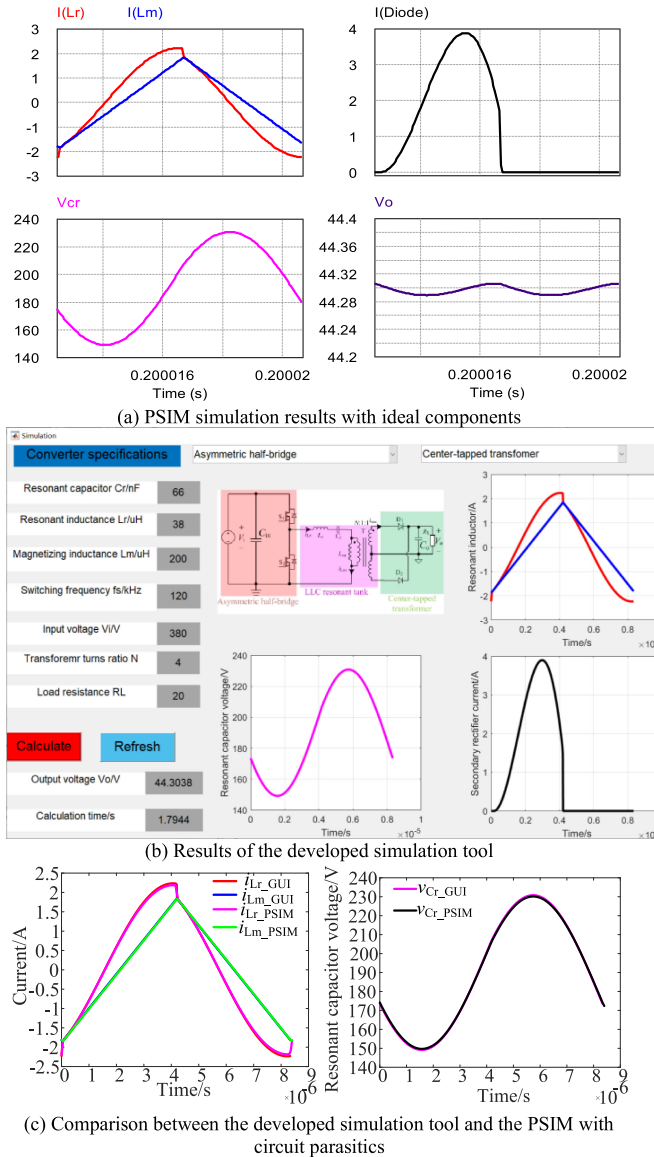


FIGURE 9. NOP operation mode.

From Figs. 11 to 14, one can observe that with the calculated switching frequency from the developed simulation tool, the desired output voltage of 48 V can be achieved under different scenarios, which validate the accuracy and effectiveness of the developed closed-loop simulation tool.

E. COMPARISON BETWEEN THE PROPOSED SIMULATION TOOLS AND THE COMMERCIAL SIMULATION SOFTWARE

It can be seen that for almost all operation modes, the calculation time is below two seconds. Please note that all these simulations are done with the same laptop (Dell Inspiron 13 with Intel core i7). The required simulation times for different simulation software with above 11 operation modes are compared as shown in Fig. 15. Please note that all these commercial simulation software are offline simulations. The ‘fsolve’

function in MATLAB is used to solve the non-linear equations for each operation mode [16]. The default trust-region dogleg algorithm is adopted. The termination tolerance of the function is set as default (1E-6) and the maximum number of iterations is also set as default (400). The simulation step for the commercial software is 20 ns to provide enough accuracy. Clearly, the proposed simulation tool is much faster than the commercial simulation software to obtain the steady state results, including fixed-step simulation (PSIM) and variable-step simulation (LTSPICE and SIMULINK). Although it is not complete fair to make comparison between the developed simulation tool and the commercial simulation software since only the steady state results can be obtained for the developed simulation tool, the following benefits of the developed simulation tools also make them attractive: 1) the important simulation waveforms, circuit voltage and current values are displayed automatically in the developed tools, which saves the time to choose and measure in the commercial simulation software. In the commercial simulation software, users have to select the circuit waveforms and measure the important values manually, which takes much more time than simulation, especially when iteration process is required; 2) for the developed simulation tool, the user only need to select the primary and secondary structures and does not need to build the circuit, which is more convenient than the commercial simulation software; 3) the developed simulation tool is more advantageous in automatic design, where massive iterations are required. The developed tool can automatically achieve the iterations and collect all the results for design and evaluation purposes.

There are two factors that are considered in the developed simulation tools to improve the execution time: 1) mode judgement; 2) initial iteration point. Firstly, as we stated previously, an improved mode judgement method is proposed in this article. Since the solver of the converter and the mode judgement is based on the initial assumption, a false assumption will lead to false calculation results and judgement. In this paper, an improved mode judgement method is carried out at an angle slightly greater than the switching angle between two stages, and the result will not output until it is consistent with the assumption. Secondly, defining the initial iteration point is also important, which would affect the calculation speed significantly. Some general principles can be applied to define the initial point: 1) the converter voltage gain m is less than unity when the operating switching frequency is higher than the resonant frequency, and it is higher than unity when the operating switching frequency is lower than the resonant frequency; 2) the resonant inductor current initial value is negative when the converter is operating in inductive region. The boundary point is when the converter operating at peak gain point, which occurs in PN or PON operation modes. Thus, except for PN and PON operations, the resonant inductor current initial value should be set negative; 3) in below resonant frequency, the duration for the P stage is around half switching cycle of the resonant frequency, thus, the initial value for the duration of P stage in below resonant

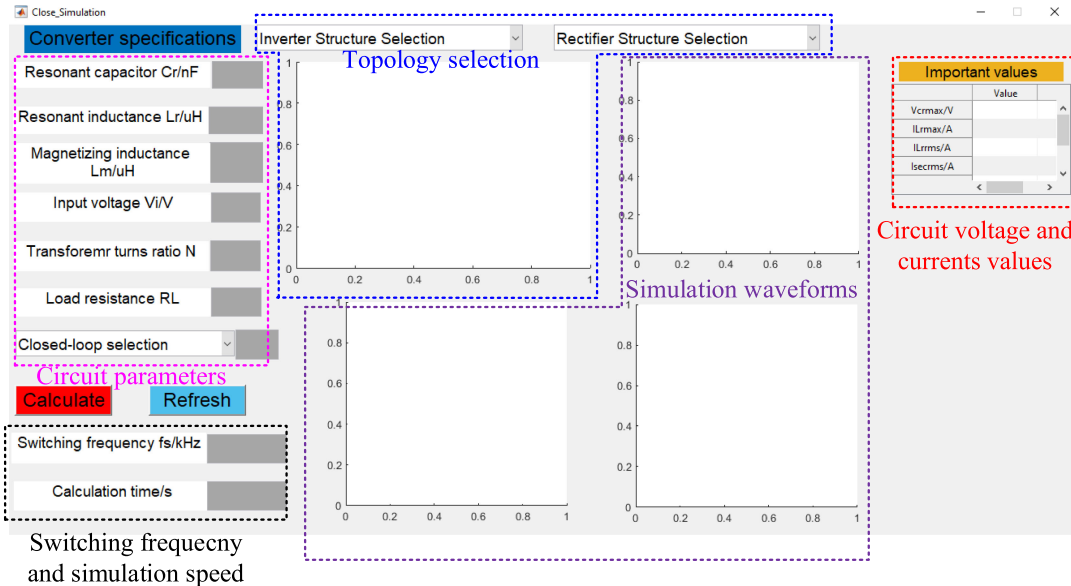


FIGURE 10. The designed MATLAB GUI program for closed-loop simulation tool.

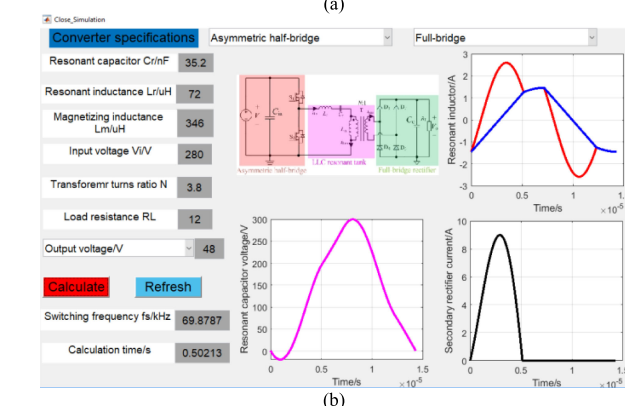
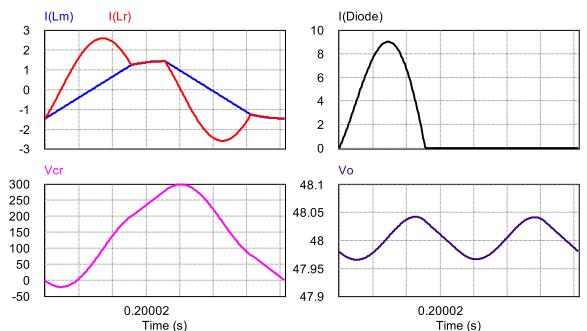


FIGURE 11. Closed-loop simulation (PO operation mode). (a) PSIM simulation results; (b) designed simulation tool results.

frequency operation modes (PN, PON, PO, and OPO) can be set around π .

V. EXPERIMENTAL RESULTS

In this Section, experiments have been conducted to validate the accuracy and effectiveness of the proposed simulation

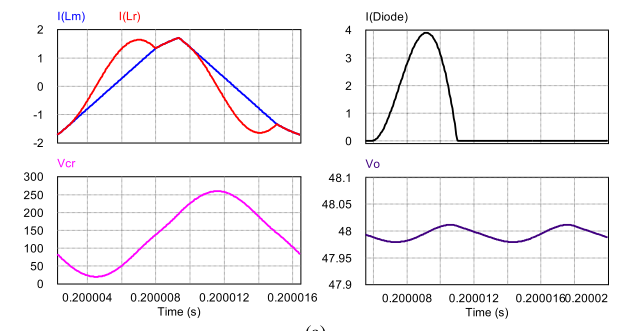


FIGURE 12. Closed-loop simulation (OPO operation mode). (a) PSIM simulation results; (b) designed simulation tool results.

tools. The circuit parameters for the experimental prototype are summarized in Table 5.

A. OPEN-LOOP EXPERIMENTAL RESULTS

Fig. 16 shows the voltage gain curve comparisons of the experimental prototype by using the proposed simulation tool, experimental results, and traditional FHA theoretical results

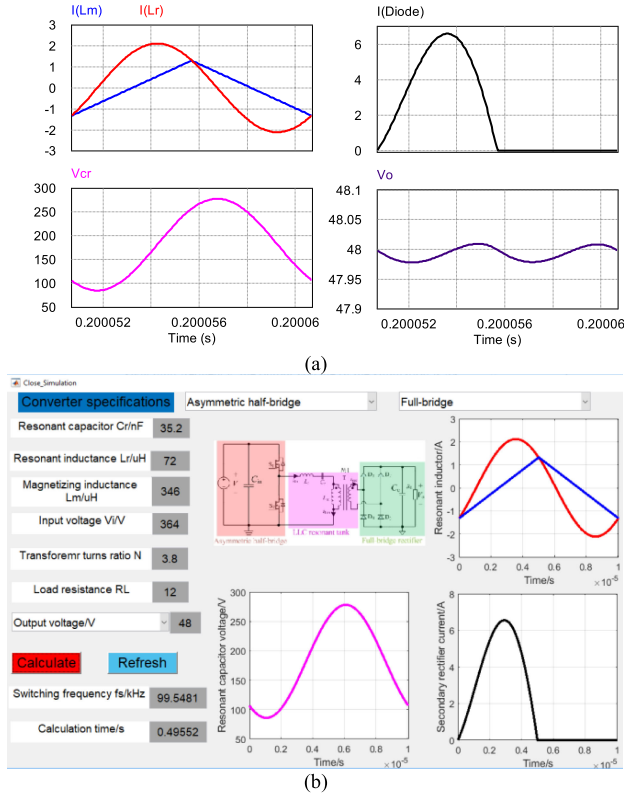


FIGURE 13. Closed-loop simulation (P operation mode). (a) PSIM simulation results; (b) designed simulation tool results.

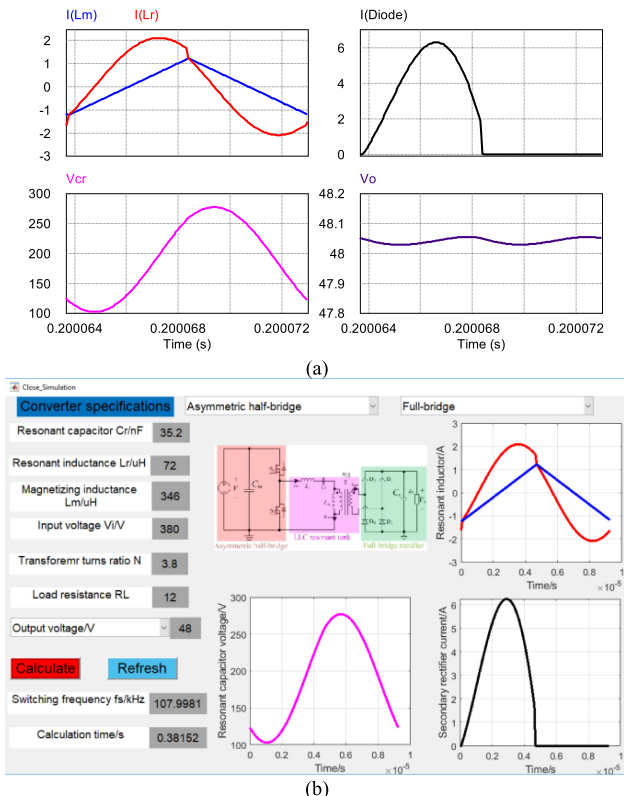


FIGURE 14. Closed-loop simulation (NP operation mode). (a) PSIM simulation results; (b) designed simulation tool results.

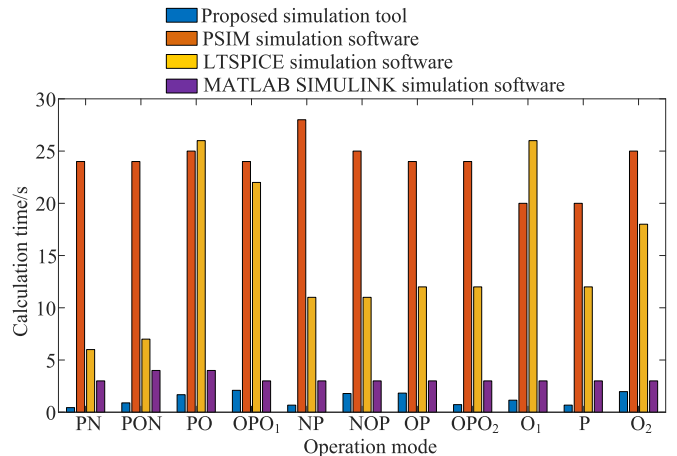


FIGURE 15. Simulation time comparisons between the proposed simulation tool and the commercial simulation software.

TABLE 5. Circuit Parameters

Components	Part number	Parameters
Resonant capacitor C_r	TDK B32621A4333J000	Two TDK film capacitors in parallel
	B32529C6222J289	33 nF/400 VDC
Resonant inductor L_r	PC44PQ32/30Z-12	72 μ H
Magnetizing inductor L_m	B66329G0000X187	EE42/20 with N87 material
Turns ratio n	EE42/20 with N87 material	Primary side 19 Secondary side 5
Output capacitor C_o	UPW2A151MHD	150 μ F/100 V
Primary switches S_1, S_2	CREE SiC MOSFET C3M0120100K	
Diode rectifier	12TQ200/S SCHOTTKY RECTIFIER	

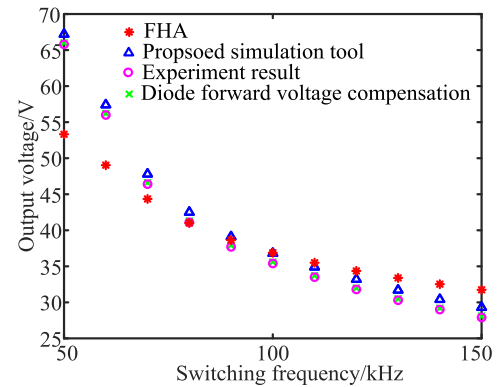


FIGURE 16. Voltage gain curve comparison.

when V_{in} equals 280 V with 12 Ω load resistor. It can be seen that traditional FHA analysis results have considerable errors when compared with the experimental results, especially when the switching frequency is away from the resonant frequency. On the other hand, the proposed simulation tool results have high accuracy, only a small mismatch exists most likely due to the voltage drops caused by circuit parasitics.

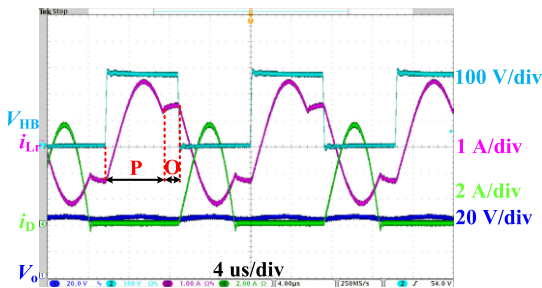


FIGURE 17. Experimental waveform at rated power with minimum input voltage.

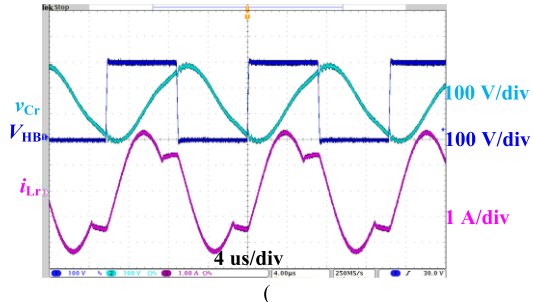


FIGURE 18. Experimental waveform of the resonant capacitor voltage.

The forward voltage drop of the rectifier diode has the largest influence. Therefore, if the diode forward voltage is compensated in the proposed simulation tool, the results are almost exactly the same as the experimental results. Therefore, the proposed simulation tool has very high accuracy.

B. CLOSED-LOOP EXPERIMENTAL RESULTS

Fig. 17 shows the closed-loop experimental waveform when input voltage equals 280 V with a $12\ \Omega$ load resistor and the output voltage is regulated at 48 V, where V_{HB} is the output voltage of the half-bridge inverter, i_{Lr} is the resonant inductor current, i_D is the rectifier diode current, and V_o is the output voltage. From the experiment waveform, we can observe that the LLC resonant converter is operating in PO operation mode. The measured switching frequency is 68 kHz, which is slightly lower than the desired minimum switching frequency due to the compensation for the voltage drops caused by the circuit parasitics. Please note that the results obtained from the designed closed-loop simulation tool are shown in Fig. 11.

Another important characteristic is the peak voltage of the resonant capacitor. Fig. 18 show the resonant capacitor voltage waveform at rated power with minimum input voltage. Clearly, the peak voltage occurs under the worst case, which is around 300 V. The resonant inductor current obtained from the theoretical analysis, simulation, and experiment are drawn in one figure as shown in Fig. 19. The simulation has the same results as the theoretical analysis, the reason is that ideal components are adopted in the simulation and parasitics are ignored. In addition, the experimental results are very close to the theoretical analysis, which can verify the accuracy and effectiveness of the proposed simulation tool.

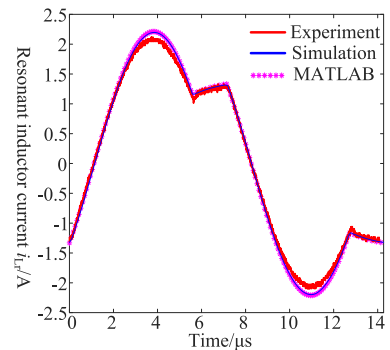


FIGURE 19. Comparison between experiment, simulation, and theoretical analysis results.

C. LIMITATIONS AND CONTRIBUTIONS OF THE DESIGNED SIMULATION TOOLS

The limitations of the designed simulation tools come from the assumption that ideal components are considered and the converter is operating in steady state condition. Therefore, the designed simulation tools cannot take circuit parasitics into considerations. In addition, the designed simulation tools can only solve the steady state operation of the LLC converters since steady state operation is one of the assumptions for the modelling. The transient operations cannot be evaluated. The transient modelling would be the focus of future work, which can help evaluate the converter dynamic performance and design the controller. Moreover, with the aid of the developed simulation tools, automatic design tool with massive iterations will be developed in the future.

For the LLC resonant converter, the major circuit parasitics include the following: 1) conduction loss related circuit parasitics, including primary MOSFET on-state resistance $R_{ds(on)}$, inductors and capacitors equivalent series resistance (ESR). These circuit parasitics influence can be simply compensated by setting a higher output voltage than the required value as we discussed before, the forward voltage drop of the rectifier diode is compensated; 2) output capacitance of primary MOSFET, this parasitic will mainly affect the zero voltage switching (ZVS) performance of the converter, which is considered as a design constraint for an LLC converter. The switch turn-off current can be accurately obtained with the designed tools and combined with the information of primary device output capacitance, the ZVS operation can be evaluated; 3) transformer parasitic capacitance and junction capacitance of secondary rectifier diode, these parasitic capacitors will have great influence on the converter voltage gain under light load operation (less than 10%-15% of load power) [17]. Generally, under light load operation, the burst mode control strategy [18] will be adopted to improve the system efficiency so that the parasitic capacitors influence on the converter can be ignored.

The contributions of this paper can be summarized as follows: 1) all operation modes are modelled and included in the simulation tools. In [7], only six operation modes (NP,

PO, OPO, NOP, PON, and PN) are included; 2) all the common circuit topologies are included in the simulation tools. The modifications for LLC converters with different structures are discussed; 3) both the open-loop and closed-loop models are discussed, and the corresponding simulation tools are designed. In the literature, only the open-loop model is discussed; 4) an improved mode judgement method is proposed. Traditionally, the boundary condition between different modes is defined by the magnetizing inductor voltage mL_m [7]. However, because of the abrupt change of the voltage at the switching angle between two resonant stages, the accuracy of the mode judgement is reduced. Since the solver of the converter and the mode judgement are based on the initial assumption, a false assumption will lead to false calculation results and judgement. In this paper, an improved mode judgement method is carried out at an angle slightly greater than the switching angle between two stages, and the result will not output until it is consistent with the assumption.

VI. CONCLUSION

In this paper, LLC resonant converter simulation tools are designed based on the MATLAB GUI. Compared with the existing literatures, the designed simulation tools have the following features and advantages: 1) all common LLC resonant converter topologies are included in the simulation tools, based on the discussion, there exist fifteen possible LLC resonant converter topologies; 2) mathematical derivations for all possible operation modes are presented, eleven operation modes including PN, PON, PO, OPO, O, P, O, NP, NOP, OP, OPO are discussed; meanwhile, the boundary conditions for different operation modes are analyzed and derived; 3) some key circuit voltage and current values are summarized in a table to facilitate the analysis and design of the LLC resonant converters, while for the commercial simulation tool, the user has to use a measurement tool to obtain this information, which can be time-consuming; 4) the calculation speed is much faster than the commercial simulation software, comprehensive comparisons between different commercial simulation software are made.

The designed simulation tools will benefit the readers and engineers in the following three aspects: 1) educational purpose: the designed simulation tools are accurate and complete, which can be used for students or beginners who are doing research in LLC resonant converters; 2) design and optimization purpose: the developed simulation tools can be used to evaluate different design candidates and finalize the circuit design; 3) verification purpose: like all other commercial simulation software, it can be used to verify the accuracy of your design and experimental results, and indicate when to make necessary modifications when conducting experiments.

REFERENCES

- [1] Y. Wei, Q. Luo, S. Chen, P. Sun, and N. Altin, "Comparison among different analysis methodologies for LLC resonant converter," *IET Power Electron.*, vol. 12, no. 9, pp. 2236–2244, Aug. 2019.
- [2] T. Liu, Z. Zhou, A. Xiong, J. Zeng, and J. Ying, "A novel precise design method for LLC series resonant converter," in *Proc. IEEE INTELEC*, 2006, pp. 1–6.
- [3] Z. Hu, L. Wang, H. Wang, Y. Liu, and P. C. Sen, "An accurate design algorithm for LLC resonant Converters—Part I," *IEEE Trans. Power Electron.*, vol. 31, no. 8, pp. 5435–5447, Aug. 2016.
- [4] Z. Hu, L. Wang, Y. Qiu, Y. Liu, and P. C. Sen, "An accurate design algorithm for LLC resonant Converters—Part II," *IEEE Trans. Power Electron.*, vol. 31, no. 8, pp. 5448–5460, Aug. 2016.
- [5] X. Fang, H. Hu, Z. J. Shen, and I. Batarseh, "Operation mode analysis and peak gain approximation of the LLC resonant converter," *IEEE Trans. Power Electron.*, vol. 27, no. 4, pp. 1985–1995, Apr. 2012.
- [6] J. Deng, C. C. Mi, R. Ma, and S. Li, "Design of LLC resonant converters based on operation-mode analysis for level two PHEV battery chargers," *IEEE Trans. Mechatronics*, vol. 20, no. 4, pp. 1595–1606, Aug. 2015.
- [7] R. Yu, G. K. Y. Ho, B. M. H. Pong, B. W. Ling, and J. Lam, "Computer-aided design and optimization of high-efficiency LLC series resonant converter," *IEEE Trans. Power Electron.*, vol. 27, no. 7, pp. 3243–3256, Jul. 2012.
- [8] Y. Wei, Q. Luo, X. Du, N. Altin, J. M. Alonso, and H. A. Mantooth, "Analysis and design of the LLC resonant converter with variable inductor control based on time-domain analysis," *IEEE Trans. Ind. Electron.*, vol. 67, no. 7, pp. 5432–5443, Jul. 2020.
- [9] A. Kumar, A. Awasthi, O. Salari, A. Laha, and P. Jain, "An exact time-domain based novel simulation-design tool for study and optimal design of LLC and CLL resonant converters," in *Proc. IEEE Energy Convers. Congr. Expos.*, 2019, pp. 673–680.
- [10] A. Kumar, A. Awasthi, O. Salari, A. Laha, A. Mathew, and P. Jain, "A time-domain based APP designer for resonant converters with GUI features," in *Proc. IEEE APEC Expo.*, 2020, pp. 2860–2867.
- [11] Y. Wei, Z. Wang, Q. Luo, and A. Mantooth, "A MATLAB GUI program for LLC resonant converter," in *Proc. 2020 IEEE Workshop Wide Bandgap Power Devices Appl. Asia*, 2020, pp. 1–5.
- [12] Y. Wei, Q. Luo, Z. Wang, and H. A. Mantooth, "A complete step-by-step optimal design for LLC resonant converter," *IEEE Trans. Power Electron.*, vol. 36, no. 4, pp. 3674–3691, Apr. 2021.
- [13] Y. Wei, Q. Luo, and A. Mantooth, "Overview of modulation strategies for LLC resonant converter," *IEEE Trans. Power Electron.*, vol. 35, no. 10, pp. 10423–10443, Oct. 2020.
- [14] W. Inam, K. K. Afzidi, and D. J. Perreault, "Variable frequency multiplier technique for high-efficiency conversion over a wide operating range," *IEEE J. Emerg. Sel. Top. Power Electron.*, vol. 4, no. 2, pp. 335–343, Jun. 2016.
- [15] Y. Wei, Z. Wang, Q. Luo, and A. Mantooth, "A fast and accurate simulation tool for LLC converters," in *Proc. IEEE APEC Expo.*, 2021, pp. 152–159.
- [16] [Online]. Available: <https://www.mathworks.com/help/optim/ug/fsolve.html>
- [17] B. Lee, M. Kim, C. Kim, K. Park, and G. Moon, "Analysis of LLC resonant converter considering effects of parasitic components," in *Proc. IEEE INTELEC*, 2009, pp. 1–6.
- [18] B. Wang, X. Xin, S. Wu, H. Wu, and J. Ying, "Analysis and implementation of LLC burst mode for light load efficiency improvement," in *Proc. IEEE APEC Expo.*, 2009, pp. 58–64.



YUQI WEI (Graduate Student Member, IEEE) was born in Henan, China, in 1995. He received the B.S. degree in electrical engineering from Yan-shan University, Qinhuangdao, China, in 2016, the M.S. degree in electrical engineering from the University of Wisconsin-Milwaukee, Milwaukee, WI, USA, in 2018, and the second M.S. degree in electrical engineering from Chongqing University, Chongqing, China, in 2019. He is currently working toward the Ph.D. degree with the University of Arkansas, Fayetteville, AR, USA.

His current research interests include wide band gap devices and active gate driving. Mr. Wei was the recipient of the 2020 IEEE Power Electronics Society Transactions Second Place Prize Paper Award.



ZHIQING WANG was born in Chongqing, China, in 1994. She received the B.S. and M.S. degrees in electrical engineering from Chongqing University, Chongqing, China, in 2017 and 2020, respectively. She is currently working with Monolithic Power Systems, Inc. Chengdu, China. Her current research interests include power converter topologies and advanced control for renewable energy systems.



H. ALAN MANTOOTH (Fellow, IEEE) received the B.S. and M.S. degrees in electrical engineering from the University of Arkansas, Fayetteville, AR, USA, in 1985 and 1986, respectively, and the Ph.D. degree from the Georgia Institute of Technology, Atlanta, GA, USA, in 1990. He then joined Analogy, a startup company in Oregon, where he focused on semiconductor device modeling and the research and development of modeling tools and techniques. In 1998, he joined the Faculty of the Department of Electrical Engineering with the University of Arkansas, where he is currently holds the rank of a Distinguished Professor. His current research interests include analog and mixed-signal IC design & CAD, semiconductor device modeling, power electronics, and power electronic packaging. He helped establish the National Center for Reliable Electric Power Transmission (NCREPT) at the UA in 2005. He is the Executive Director for NCREPT and also two of its centers of excellence: the NSF Industry/University Cooperative Research Center on GRid-connected Advanced Power Electronic Systems (GRAPES) and the Cybersecurity Center on Secure, Evolvable Energy Delivery Systems (SEEDS) funded by the U.S. Department of Energy. In 2015, he also helped to establish the UA's first NSF Engineering Research Center entitled Power Optimization for Electro-Thermal Systems (POETS) that focuses on high power density systems for transportation applications. He holds the 21st Century Research Leadership Chair of engineering. He is the Immediate Past-President of the IEEE Power Electronics Society during 2019–2020 and the Editor-in-Chief of IEEE OPEN JOURNAL OF POWER ELECTRONICS. He is a member of Tau Beta Pi and Eta Kappa Nu, and registered a Professional Engineer in Arkansas.



QUANMING LUO (Member, IEEE) was born in Chongqing, China, in 1976. He received the B.S., M.S., and Ph.D. degrees in electrical engineering from Chongqing University, Chongqing, China, in 1999, 2002, and 2008, respectively. From 2002 to 2005, he was with the Emerson Network Power Co. Ltd., Shenzhen, China, as a Research and Development Engineer. Since 2005, he has been with the College of Electrical Engineering, Chongqing University, where he is currently a Professor. His current research interests include LED driving systems, communication power systems, power harmonic suppression, and power conversion systems in electrical vehicles.